Monthly Notices of the ROYAL ASTRONOMICAL SOCIETY

MNRAS **511,** 5385–5395 (2022) https://doi.org/10.1093/mnras/stac116
Advance Access publication 2022 February 11

Plateaus, dips, and rebrightenings during the outbursts of WZ Sge: no magnetic propeller, but a veiling curtain

M. Georganti [1]★ C. Knigge,[1] N. Castro Segura [1] and K. S. Long[2,3]

[1] *Department of Physics and Astronomy, University of Southampton, Southampton, Hampshire, SO17 1BJ, UK*
[2] *Space Telescope Science Institute, 3700 San Martin Drive, Baltimore, MD 21218, USA*
[3] *Eureka Scientific, Inc. 2452 Delmer Street, Suite 100, Oakland, CA 94602-3017, USA*

Accepted 2022 January 5. Received 2021 December 23; in original form 2021 August 6

ABSTRACT

WZ Sge is the prototype of highly evolved, low-accretion rate dwarf novae (DNe). During the decline from eruptions, its light curve displays a 'dip' followed by $\simeq$10 'echo outbursts'. The standard disc instability model does not account for this behaviour, which is also seen in other low-accretion rate DNe. One recent interpretation for these rapid brightness changes is that they represent transitions into and out of a magnetic propeller regime. Here, we test this scenario with time-resolved, ultraviolet spectroscopy taken with the *Hubble Space Telescope* just before, during and after the dip in *WZ Sge*'s 2001 eruption. We find no distinctive or unique signatures that could be attributed to a propeller in either the time-averaged UV spectrum or the variability spectrum. Thus the data do not support the magnetic propeller scenario. Instead of resolving the mystery of *WZ Sge*'s outburst light curve, our study has actually added another: the origin of the narrow absorption features seen in all outburst phases. We show explicitly that these features are likely formed in a high-density 'veiling curtain' with a characteristic temperature $T \simeq 17,000$ K. However, the nature and origin of this veil are unclear. Given that *WZ Sge*-type DNe are the most intrinsically common class of accreting white dwarfs, resolving these questions should be a high priority.

Key words: accretion – accretion discs – magnetic fields – stars: dwarf novae – stars: individual: WZ Sge.

1 INTRODUCTION

Dwarf novae (DNe) constitute one subclass of cataclysmic variables (CVs), where a late, low-mass ($\leq$1 $M_\odot$) Roche lobe filling star transfers mass to a white dwarf (WD) primary through the formation of an accretion disc. One of the most extensively studied CVs—and our focus in this paper—is the DN *WZ Sge*. This system is one of the closest CVs (d = 45.2 ± 0.1 pc − Gaia Collaboration 2021) and – with an orbital period of 82 min and a donor at or below the Hydrogen-burning limit (e.g. Patterson 2001; Patterson et al. 2005; Steeghs et al. 2007)—also one of the most highly evolved. As the prototype of its own subcategory of low-accretion rate DNe (e.g. Lasota, Hameury & Huré 1995; Kato 2015), the *WZ Sge*-type systems, *WZ Sge* presents spectacular high-amplitude ($\simeq$7 mag) extended super outbursts with a recurrence time-scale in the range of decades ($\simeq$30 yr).

The standard theoretical framework used to describe the eruptions of DNe is the disc instability model (DIM; e.g. Osaki 1996; Lasota 2001; Hameury 2020 for recent reviews). The DIM assumes that the mass-transfer rate from the companion star remains approximately constant. During quiescence, most of the mass transferred from the secondary accumulates in the accretion disc. An outburst is triggered when the surface density reaches a critical value at some radius. This sets off a Hydrogen ionization instability and launches a heating wave across the disc. The viscosity and mass-transfer rate through the disc then both increase, causing the system to brighten dramatically. Near the peak of an outburst, the mass-transfer rate through the disc is higher than the rate at which mass is added to the outer disc by the donor star. Eventually, therefore, another critical surface density is reached, and the disc transitions back to the mostly neutral quiescent state via a cooling wave.

The *WZ Sge* stars typically undergo only *super* outbursts, which are brighter and longer than normal outbursts. Some additional physics is needed in order to explain the existence of both types of eruptions, such as an increase in viscosity when the disc reaches the 3:1 resonance radius (Osaki 1989, 1995), or a combination of irradiation, mass-transfer rate variations and disc truncation (Hameury, Lasota & Warner 2000a). In *WZ Sge* specifically, inner disc truncation in quiescence is certainly plausible, since coherent, fast optical (Robinson, Nather & Patterson 1978; Patterson 1980), and X-ray (Patterson et al. 1998) oscillations point to a rapidly rotating (P_{spin} = 27.87 s) magnetic WD.

However, almost all *WZ Sge* stars exhibit a distinct and complex light curve pattern after their super-outburst peak, comprised of a 'dip' and subsequent 'echo outbursts' (aka 'rebrightenings') before their luminosity reaches again the quiescent level. This paper particularly investigates *WZ Sge*'s 2001 super outburst, during which these phases were clearly apparent (Fig. 1). These features are not explained by any of the standard DIM flavours.

Against this background, Campana et al. (2018) recently proposed that distinctive luminosity drops ('dips' or 'knees') during the outburst decay of many different types of accreting systems – from low-mass and high-mass X-ray binaries to CVs and young stellar objects – may all be explained by a single unifying framework. In their picture, these dips signal a temporary transition to a magnetic

★ E-mail: M.Georganti@soton.ac.uk

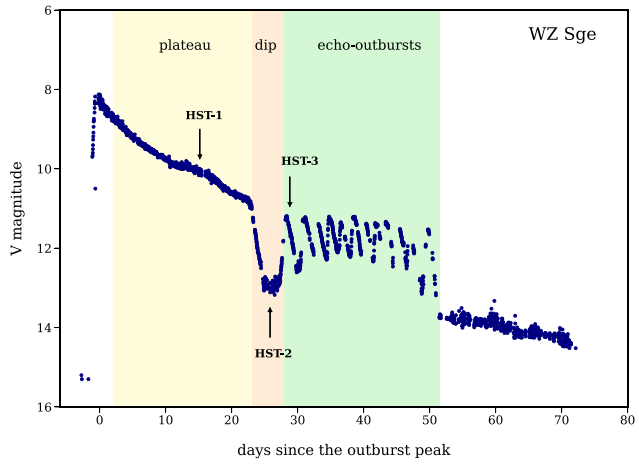

Figure 1. VSNET optical light curve of *WZ Sge*'s 2001 super outburst with respect to days since its outburst peak (Ishioka et al. 2002). Three different regions, at the outburst decay, are background highlighted: the plateau (yellow), the dip (orange), and the echo-outburst phase (green). The times of our *Hubble Space Telescope (HST)* observations are marked by arrows and cover all the decline stages of the super outburst.

propeller state, in which the magnetic accretor rotates faster than the inner edge of the disc. This creates a centrifugal barrier, so material reaching the inner disc cannot accrete by latching on to magnetic field lines and is ejected instead.

In order to test Campana et al.'s (2018) scenario for *WZ Sge* (and similar systems), our strategy is to compare far-UV and near-UV spectra of the system obtained before, during and after the 'dip' in its outburst light curve (Fig. 1). If the system enters a propeller state during the dip, we would expect this to produce strong changes in the UV spectrum.

What kind of spectral and variability signatures may we expect during a propeller phase? Among WD binaries, the only well-established magnetic propeller system is *AE Aqr* (e.g. Eracleous et al. 1994; Eracleous & Horne 1996; Wynn, King & Horne 1997), although a second candidate, *LAMOST J024048.51+195226.9 (J0240)*, has recently been discovered (Garnavich et al. 2021). *AE Aqr* is not known to undergo DN eruptions and instead seems to be in a permanent propeller state that gives rise to a host of unusual observational properties (e.g. Meintjes, Oruru & Odendaal 2012). One of these properties is strong, aperiodic flaring activity on time-scales of minutes. These flares are thought to be associated with shock-heated 'fireballs' (Pearson, Horne & Skidmore 2003) produced when blobs of material are violently ejected from the magnetosphere (Eracleous & Horne 1996) and/or when ejected blobs collide with each other (Welsh, Horne & Gomer 1998). The recent discovery that flaring activity is suppressed during eclipses in *J0240* tends to support the former scenario.

The fireballs produced by the magnetic propeller in *AE Aqr* also give rise to an extremely distinctive emission line spectrum (Pearson et al. 2003). As shown in Fig. 2, in the far-UV (<2000 Å) region, the spectrum is characterized by strong, broad, and single-peaked lines associated with a wide range of ionization states and densities. High-density, high-ionization lines include N V λ1240 Å, Si IV λ1400 Å, He II λ1640 Å, while the lower-density, lower-ionization transitions include O III] λ1663 Å and Si III] λ1892 Å. In the near-UV (>2000 Å) range, aside from the prominent Mg II line, the main feature is a strong, broad complex associated with Fe II.

Is *AE Aqr* a reasonable 'template' for what *WZ Sge* might look like in a propeller state? There are at least three areas of concern. The first is that the material that is accreted/ejected in *AE Aqr* is supplied by an evolved donor star and has therefore undergone CNO processing. This naturally gives rise to anomalous line ratios (Mauche, Lee & Kallman 1997; Gänsicke et al. 2003), with, for example, N V λ1240 Å being stronger than C IV λ1550 Å. However, fireballs are expected to produce strong and distinctive emission line spectra even for quite extreme abundance variations (Pearson et al. 2003).

A second concern is that the accretion-heated WD in *WZ Sge* could conceivably swamp the time-averaged propeller signature in the UV. This can be mitigated by focusing on the spectrum of the *variable* component. Given the strong variations associated with the propeller signature in *AE Aqr*, this should allow a more sensitive test for the presence of the same signature in *WZ Sge*.

However, the third and most serious issue is that propellers in the two systems might produce different observational signatures because they are fed differently. More specifically, *WZ Sge* clearly harbours an accretion disc, whereas there is no observational evidence for a disc in *AE Aqr*, and none is included in the 'standard propeller model' outlined above. However, recent magneto-hydrodynamical simulations suggest a (transient, highly variable) disc may actually be present in *AE Aqr* (Isakova et al. 2016; Blinova et al. 2019). Moreover, there is at least one disc-accreting compact binary system that exhibits the same distinctive UV spectral signatures as *AE Aqr*—the transitional millisecond pulsar *PSR J1023+0038 (J1023)* (Hernández Santisteban 2016). In this system, the inner disc appears to be truncated and ejected by the pulsar wind at a distance from the accretor that is comparable to the magnetospheric radius of *AE Aqr* (Hernández Santisteban 2016). This suggests that similar UV spectra can be produced regardless of the details of the ejection mechanism, provided that key parameters—such as the mass-transfer rate and ejection radius—are comparable. In this sense, *WZ Sge* is actually quite a good match to *AE Aqr*. Both appear to harbour moderately massive ($M_{WD} \simeq 0.63\ M_\odot$ – Echevarría et al. 2008) and fast-spinning ($P_{spin} \simeq 30$ s – e.g. Patterson 1979; Patterson et al. 1998) WDs, and the mass-transfer rates near the inner disc edges are also comparable. In *AE Aqr*, this rate is set by the secondary star ($\dot{M}_{tr} \simeq 10^{-9}\ M_\odot\ yr^{-1}$ – Eracleous & Horne 1996). In *WZ Sge*, the donor feeds the disc at a much lower rate ($\dot{M}_2 \simeq 10^{-11}\ M_\odot\ yr^{-1}$ – e.g. Smak 1993), but the transfer rate *through the inner disc* near the end of the plateau phase is also $\dot{M}_{tr} \simeq (1-3) \times 10^{-9}\ M_\odot\ yr^{-1}$ (Long et al. 2003).

Given all this, we will refer to *AE Aqr*'s UV spectrum as a convenient reference point, but consider *any* unique or distinctive spectral signature in the dip phase as a potential propeller signature. As we shall see, there is no such signature in our observations, i.e. no sign of a magnetic propeller. However, somewhat unexpectedly, all of our spectra show evidence for the presence of an absorber that veils the underlying continuum. Presumably the same veiling material was highlighted by Long et al. (2004) in the WD-dominated spectra taken later during the same outburst. However, our data show that the absorber is already present much earlier, during the disc-dominated phases of the eruption. We characterize the physical properties of this curtain, but its origin in the system remains uncertain.

2 OBSERVATIONS AND DATA ANALYSIS

2.1 Observations: UV Spectroscopy with *HST*

WZ Sge was observed on 2001 August 8, 19, and 22 after its eruption peak on July 24 (Ishioka et al. 2002), with the aim of studying the immediate aftermath and decline phase of its super outburst. The observations (Proposal ID: 9287, PI: Knigge) were obtained with the

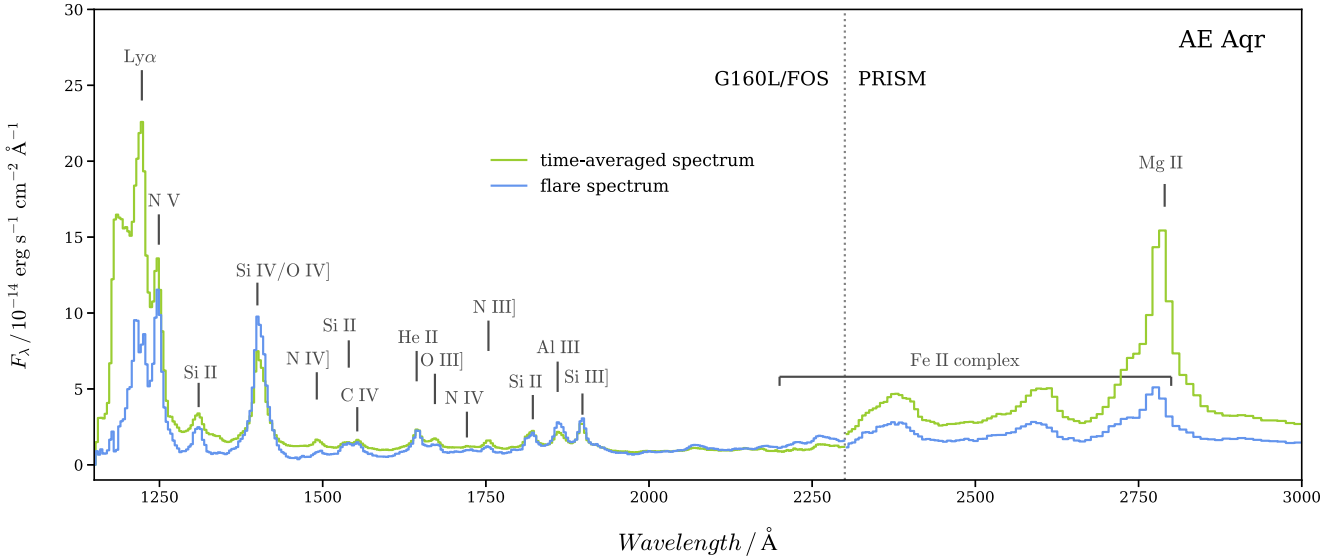

Figure 2. UV time-averaged (light green) and flare/variability (light blue) spectra of *AE Aqr* (Eracleous et al. 1994; Eracleous & Horne 1996). The spectra between 1150–2300 Å are obtained by using the G160L grating of the *Faint Object Spectrograph* (*FOS*) on board the *HST* whereas their 2300–3000 Å part is acquired by exploiting *PRISM*. It can be seen that, at the blue part of the spectrum, a wide range of ionization states and semi-forbidden emission lines are discernible while at the red part, only the Fe II complex and the Mg II line are clearly visible.

Space Telescope Imaging Spectrograph (*STIS*) on board the *HST* and retrieved from the Mikulski Archive for Space Telescopes (MAST).

In the far-UV, all of the spectra of *WZ Sge* were acquired with the photon-counting FUV-MAMA detector operating in TIME-TAG mode, providing photon arrival times with a relative accuracy of 125 μs. The E140M/1425 Å echelle grating was used to obtain the spectra between the wavelength range 1144–1710 Å with a spectral resolution of R = 45 800 – this resolution corresponds to a velocity resolution of ≃7 km s^{-1}. In the near-UV, our spectra (ranging between 1605–3110 Å) were obtained by the NUV-MAMA detector, operating in ACCUM mode. This set of observations exploited the E230M/1978 Å and E230M/2707 Å grating, offering the spectral resolution of R = 30 000 – corresponding, respectively, to a velocity resolution of ≃10 km s^{-1}. The 0.2 arcsec × 0.06 arcsec slit was used for the plateau phase and the 0.2 arcsec × 0.2 arcsec slit for the other two epochs. Each epoch is consisted of a single four-orbit visit with *HST* orbits and (somewhat fortuitously) covered three key points in the outburst: the 'plateau' (*HST*-1), the 'dip' (*HST*-2), and the 'echo-outburst' phase (*HST*-3). Fig. 1 shows the timing of these observations superposed on *WZ Sge*'s 2001 super-outburst optical light curve.

On the other hand, the *AE Aqr* spectra were acquired over nine *HST* orbits on 1992 November 27–28 (Eracleous et al. 1994; Eracleous & Horne 1996). During the first eight orbits, the G160L grating of *FOS* on board the *HST* was used, covering the range of 1150–2510 Å with a spectral resolution of 9.2 Å (FWHM). In the last orbit though, the G160L grating was replaced by *PRISM*, instrument that covers the spectral range between 1500–6015 Å and is characterized by a low and variable spectral resolution (e.g. 44 Å at Mg II λ2800 Å, 92 Å at Balmer edge and 140 Å at Hγ; Sirk & Bohlin 1986; Evans 1993). The much lower resolution of the *FOS* instruments has to be taken into account in comparing the two sources, of course. However, the key point for our study is that the emission lines in the G160L range are *resolved* and thus are definitely broad. For example, the FWHM of the He II λ1640 Å line, corrected for the instrumental resolution, is ≃1700 km s^{-1} (Eracleous & Horne 1996).

2.2 Data Analysis

We first constructed wavelength-integrated light curves from the time-resolved observations using the LIGHTCURVE package.[1] This process included both background subtraction and removal of time windows affected by buffer dumps. Rapid variability was present during all stages, as demonstrated in Fig. 3. A search for periodic variability in these data sets was already carried out by Knigge et al. (2002), finding evidence for ≃14 s oscillations (only) in the third epoch (*HST*-3).

One peculiar feature in the plateau phase light curve (upper panel of Fig. 3) is the drop in the count rate between the first and second orbit (1 → 2) and again between the third and fourth one (3 → 4). In both cases, this drop is followed by a slow recovery of the count rate back to its previous level. We suspect that this is an artefact, probably due to the object moving in and out of the very small slit used (only) in this epoch. That said, inspection of the target acquisition and jitter files did not reveal any obvious long term drifts. In order to test this suspicion, we have extracted spectra separately for the first and second halves of the second and fourth orbits of the plateau phase. As expected from variability induced by the target moving within the slit, the ratios of these spectra are almost flat, with sharp, narrow 'P-Cygni'-like features that are likely due to movement in the dispersion direction. We have also checked that this is not the case for the stochastic variability seen, for example, in orbit 4 of the dip phase. Here, the ratio of spectra extracted from high and low count rate states essentially looks like the transmission spectrum of the 'veil' discussed in Section 3.2. We conclude that the slow variability in the plateau phase was indeed likely due to target motion within the slit, but that the remaining stochastic variability in this and other epochs is intrinsic to the source.

We then constructed both mean and variability (RMS) UV spectra of *WZ Sge*. The purpose of the RMS spectra is to isolate features that

[1] source: https://github.com/justincely/lightcurve.

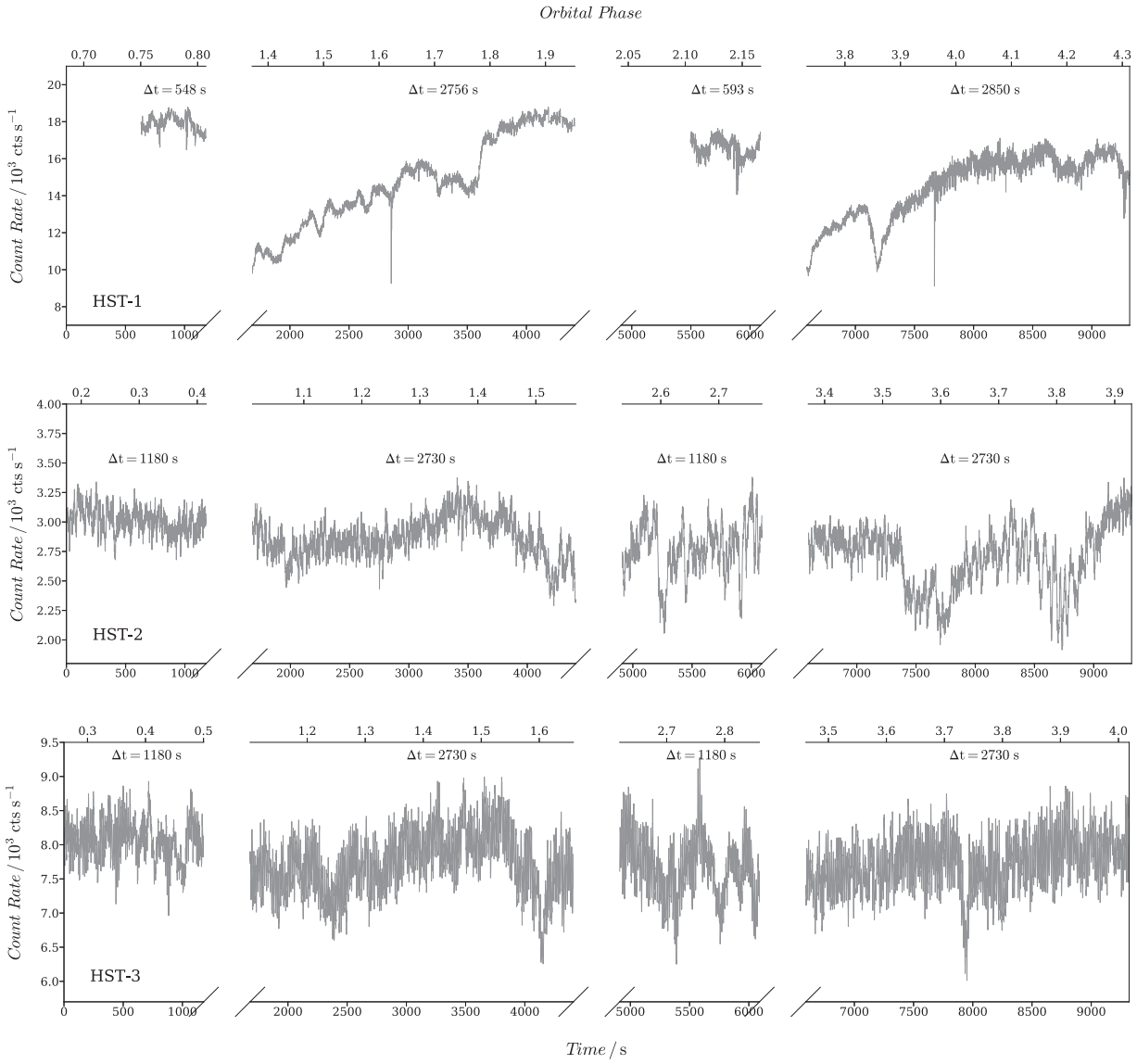

Figure 3. Extracted one-second resolution light curves of *WZ Sge* for the three studied epochs, each one of them composed of four different orbits. The duration of each orbit as well as the orbital phase of the system are noted. The orbital phase was calculated by exploiting the ephemeris given by Patterson et al. (1998). The broken axes specify time discontinuity between the observations. The name of each epoch is indicated by using the *HST*-1 ('plateau'), *HST*-2 ('dip'), and *HST*-3 ('echo-outburst') scheme.

exhibit strong time variations (such as propeller signatures) from those that do not (such as the spectrum of the WD). In order to create the RMS spectra, we first extracted time-resolved spectra at a resolution of Δt=60 s. We then binned these spectra to 1 Å and calculated the RMS around the time-averaged mean flux for each wavelength bin separately. We checked that these particular choices for time and wavelength resolution do not significantly affect our results.

We note that features in RMS spectra cannot be interpreted like those in 'normal' spectra. Most importantly, they do not immediately distinguish between variable absorption and variable emission – *any* excess variability that is localized in wavelength will give rise to an 'emission line' in an RMS spectrum. Thus, 'P-Cygni' or 'inverse P-Cygni' features in an RMS spectrum cannot be taken as outflow or inflow signatures, for example. Instead, they are most likely the result of velocity shifts between spectra. It is also worth noting in this context that the RMS spectrum for the plateau phase may be affected by the slit-motion-induced variability noted above.

As an additional way to test for time-variable propeller signatures, we also carried out a linear decomposition of the time-resolved spectra for each epoch [$F_{obs}(t, \lambda)$] into constant [$C(\lambda)$] and variable [$V(\lambda)$] components, i.e. $F_{obs}(t, \lambda) = C(\lambda) + D(t)\,V(\lambda)$. Here, D(t) is the driving light curve for the variable component, for which we adopted a scaled and slightly smoothed version of the far-UV continuum light curve (estimated from the wavelength interval 1450 – 1500 Å). This is the same model that was used by Eracleous & Horne (1996) to construct the far-UV spectrum of flares in *AE Aqr*, although our implementation uses an unbinned maximum likelihood fit that allows us to work directly with the TIME-TAG photon stream. This method also allows to correct for the slit-motion-induced variability in the plateau phase. Specifically, in the analysis of orbits 2 and 4 in this phase, we correct the light curves at each wavelength for the slow

drift in count rate that is likely due to the motion of the target in the slit. The variable component inferred for this phase should therefore still be reliable, modulo sharp features that may be associated with movement in the dispersion direction.

Since the form of D(t) is uncertain to (at least) within a DC offset and an overall scaling, there is an unavoidable mathematical degeneracy between C(λ) and V(λ). More specifically, the inferred C(λ) will, in general, be a linear combination of the 'true' constant and variable components. By contrast, the inferred V(λ) is always just a scaled version of the 'true' variable component – i.e. its spectral shape and absorption/emission lines will always be correct (to the extent the model itself is valid, of course). As an additional tracer of the variability spectrum – one that distinguishes between emission and absorption lines and can be directly compared to the flare spectrum of *AE Aqr* – we will therefore also show V(λ) alongside the RMS spectra for each epoch.

3 RESULTS AND DISCUSSION

3.1 Properties and implications for the propeller model

The mean and RMS spectra for each epoch, along with the constant and variable components suggested by the linear decomposition, are shown in Figs 4 and 6, respectively. For comparison, the mean and flare spectra of *AE Aqr* are also shown in the bottom panels of these figures. As explained in Section 2.2, the different appearances of the RMS and variable component spectra are expected, since RMS spectra cannot be interpreted like 'normal' spectra. For example, the 'inverse P-Cygni' profiles in the RMS spectrum obtained in the dip phase (*HST*-2) are not a signature of inflow, but are most likely due to radial velocity variations in these lines.

The mean far-UV spectra in all epochs are characterized by blue continua (Fig. 4), and there is good agreement between the mean spectra and the constant component inferred from the decomposition. The continuum flux level (measured at 1450 Å) drops from 5×10^{-12} erg s^{-1} cm^{-2} Å^{-1} during the plateau phase to 7×10^{-13} erg s^{-1} cm^{-2} Å^{-1} in the dip, before rising again to a value of 1.7×10^{-12} erg s^{-1} cm^{-2} Å^{-1} during the first echo outburst.

We broadly see the same set of atomic transitions in all of our observations, almost all of them in absorption, rather than emission. These absorption lines are intrinsically quite narrow (FWHM $\simeq$ 550 km s^{-1}) and cover a fairly wide range of ionization states such as Silicon (e.g. Si II λ1263, 1527, 1533 Å, Si III λ1299 Å or Si IV λ1400 Å) and Carbon (e.g. C I λ1658 Å, C II λ1335 Å, and C IV λ1550 Å). On the other hand, there are also some weak emission features seen during the plateau and echo-outburst phases, such as the ones of N V λ1240 Å and C IV λ1550 Å (P-Cygni profiles). These are likely formed in an accretion disc wind that is driven from the system during periods when the mass-transfer rate through the disc is high (Rosen et al. 1998).

In addition, Fig. 5 shows the near-UV time-integrated mean spectra for each of our three epochs. As noted in Section 2.1, the near-UV observations were taken in ACCUM, rather than TIME-TAG mode, so no timing information is available in this band. At the blue end of the near-UV range, we see several lines associated with moderate ionization states (e.g. N IV λ1721 Å and Al III λ1860 Å) as well as some semi-forbidden ones (e.g. O III] λ1672 Å and N III] λ1754 Å), which suggests the existence of lower density line-forming regions. At longer wavelengths, we clearly see the strong double-peaked Mg II absorption line, as well as a few lines associated with the Fe II complex between 2200–2800 Å. Particularly, Fig. 5 indicates the stronger multiplets in this wavelength range: UV1 (2600–2629 Å), UV2 (2383–2405 Å), UV3 (2344–2345 Å), UV64 (2563–2595 Å). Nevertheless, all of the features we see in the near-UV are narrow absorption lines, similar to the pattern we see in the far-UV part of the spectrum.

At the risk of stating the obvious, none of the spectra we have constructed for *WZ Sge* resembles those seen in *AE Aqr*. More generally, the data do not appear to support the propeller model for the dips in the light curves of *WZ Sge* stars. First, none of the features seen in either the mean or the variability spectrum of *WZ Sge* in the dip phase are exclusive to this phase. If the system was in a propeller phase (only) during the dip, we would expect to see a distinctive line spectrum in this phase, including features associated with shock-excited emission produced during blob–blob or blob-magnetosphere collisions (Eracleous & Horne 1996; Welsh et al. 1998; Pearson et al. 2003). Secondly, all of the lines we observe in the dip phase are seen in absorption, whereas *AE Aqr* exhibits strong, highly variable emission lines. Thirdly, all of the absorption features observed in *WZ Sge* are narrow (FWHM $\simeq$ 550 km s^{-1} both in the far- and near-UV), by contrast to the broad, emission lines expected from propeller kinematics and seen, for example, in *AE Aqr* (FWHM $\simeq$ 1700 km s^{-1} – Eracleous & Horne 1996).[2] Since these considerations apply to both the mean/constant and RMS/variability spectra, masking of an underlying propeller signature by the hot WD in *WZ Sge* is also unlikely.

3.2 The origin of the narrow absorption lines

Even though we have not found the line signatures expected from a magnetic propeller, it is important to note that we do see unexpected features. As noted above and shown in Figs 4 and 6, *all* of the spectra – i.e. the mean/constant and RMS/variability spectra throughout the plateau, dip and rebrightening phases – exhibit narrow (FWHM $\simeq$ 550 km s^{-1}), mostly low-ionization absorption features. Similar features were highlighted by Long et al. (2004) in their analysis of UV spectroscopy obtained later on during the decline from outburst. Their earliest spectrum was obtained on 2001 September 11, roughly three weeks after the final epoch considered here. That date coincided with the dip between the last two echo outbursts associated with the 2001 eruption (Godon et al. 2004). The remaining spectra analysed by Long et al. (2004) were all obtained on the final decline back towards quiescence. Narrow UV absorption lines have also been seen in quiescence (Steeghs et al. 2007).

We have measured the velocity offsets of several relatively isolated narrow absorption lines (Si IV λ1393.76 Å, Si IV λ1402.77 Å, Si II λ1533.43 Å) from their rest wavelengths in the time-averaged spectrum for each of the three epochs. These turn out to be $\simeq -73 \pm 3$ km s^{-1}, which is consistent with the systemic velocity of the binary system (-72 ± 2 km s^{-1}; Spruit & Rutten 1998; Steeghs et al. 2001). However, it is worth noting that the narrow UV absorption lines seen in quiescence by Steeghs et al. (2007) were centred on -16 ± 4 km s^{-1}. The difference between this and the systemic velocity was attributed to the effect of gravitational redshift. The narrow absorption lines in our data are closer to the systemic velocity, suggesting that the line-forming region was located further from the WD.

[2]Note that the narrow absorption features we see in WZ Sge would probably not be detectable – and certainly not resolved – in the FOS spectrum of AE Aqr.

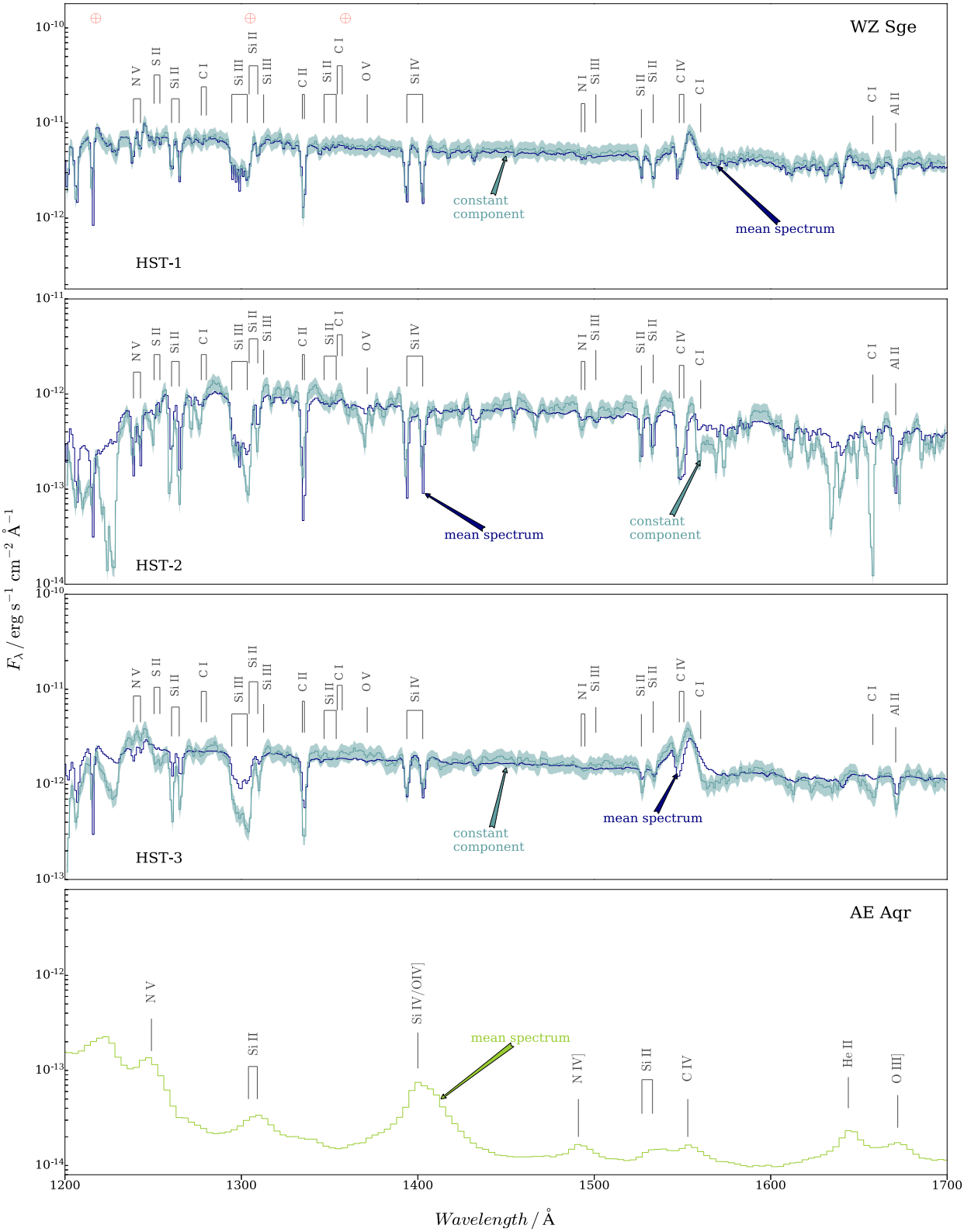

Figure 4. Flux-calibrated far-UV mean spectra (navy) for all of our epochs, plotted with respect to the constant component (teal), suggested by our linear decomposition model. The teal-shaded area corresponds to 20 per cent of the constant component's flux in both directions.The line identifications, including the geocoronal species − represented by ⊕, are shown on top of these plots. The last panel indicates the mean *AE Aqr* spectrum for comparison.

In order to characterize the conditions under which these lines must be formed, Long et al. (2004) considered a simple model in which they are produced by absorption in a slab of material with electron density $N_e \simeq 10^{11}$ cm^{-3} in local thermodynamic equilibrium (LTE). This model does a reasonable job of producing most of the observed features and provides some important insights. Specifically, they found that the temperature of their model slab decreased from T ≃ 11, 500 K in September to ≃7200 K in October, to ≃6500 K at

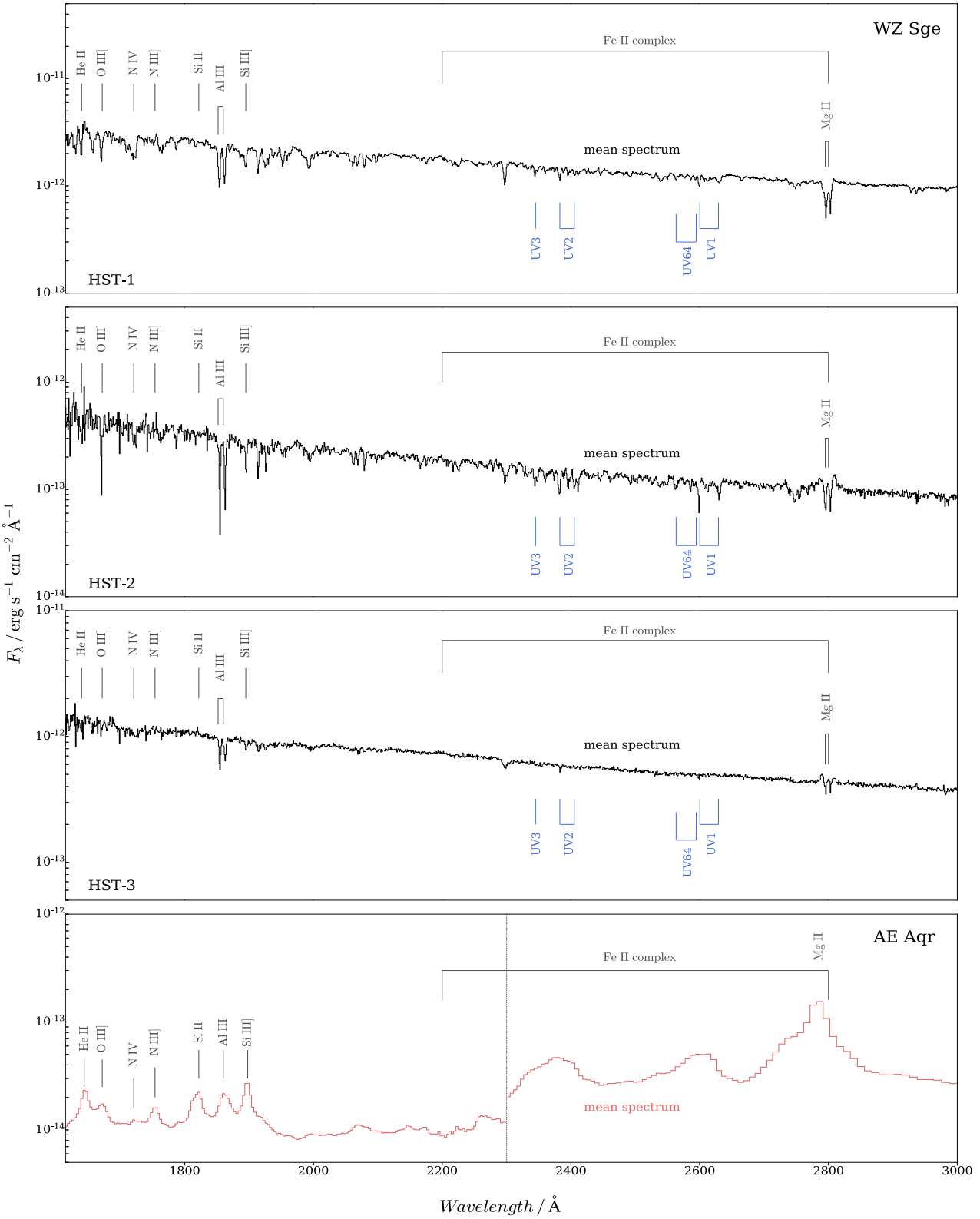

Figure 5. Near-UV mean spectra of *WZ Sge* (dark grey) for all our epochs along with the most prominent line identifications. At longer wavelengths, we identify the stronger iron multiplets (UV1, UV2, UV3, UV64). The last panel again demonstrates the mean *AE Aqr* spectrum for comparison. It is noted that we keep the distinction, presented in Fig. 2, where the 1600–2300 Å part of the spectrum is obtained by the G160L/*FOS* instrument whereas the 2300–3000 Å part of the spectrum is acquired by *PRISM*.

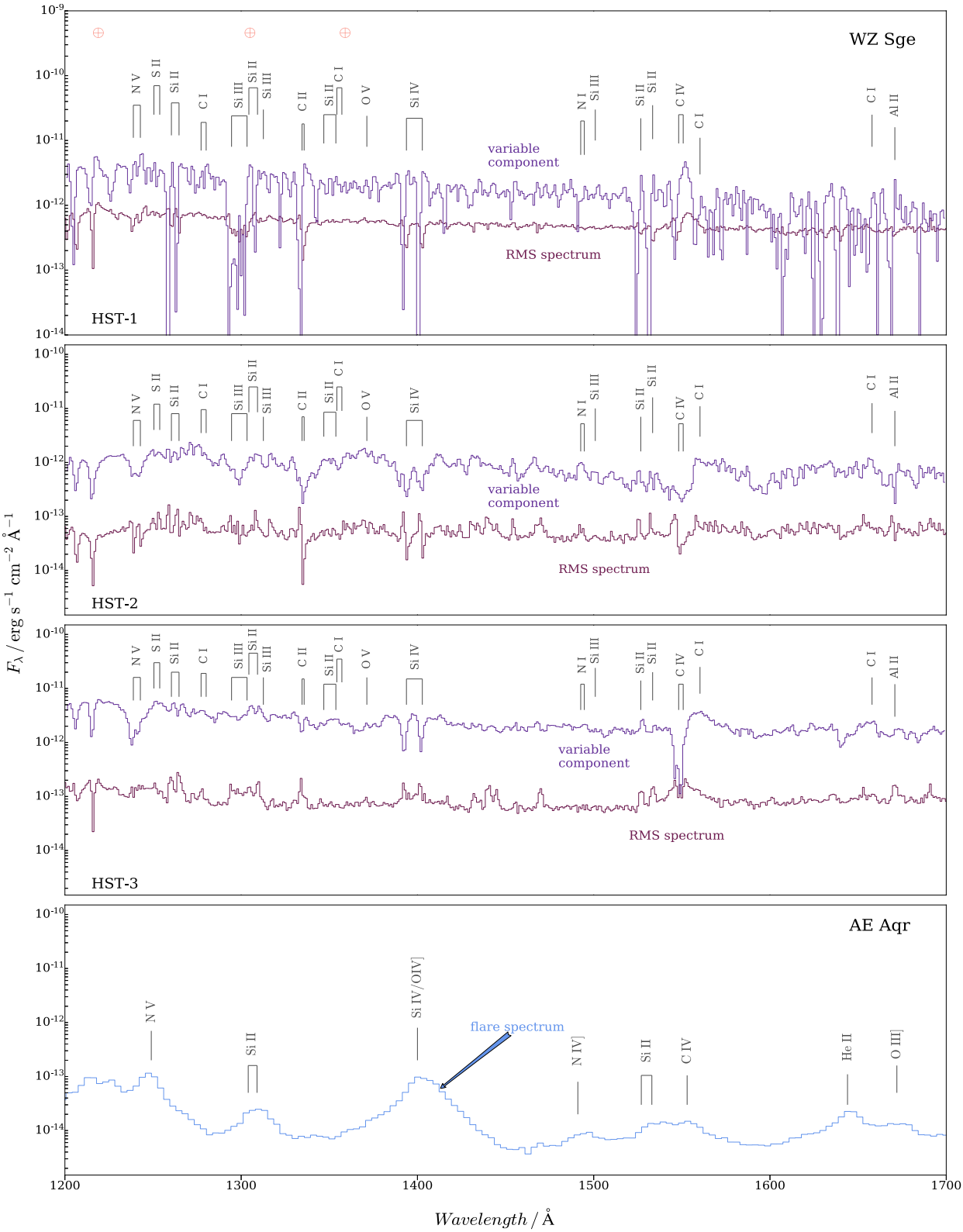

Figure 6. Flux-calibrated far-UV RMS spectra (dark magenta) for our three epochs plotted with respect to the variable component (purple) of our linear decomposition. The line identifications, including the geocoronal species – represented by ⊕, are shown on top of these plots. The last panel indicates the flare *AE Aqr* spectrum for comparison.

later times. Across the same interval, the column density of the absorber dropped from log $N_H \simeq 21.3$ to $\simeq$19.5 to $\simeq$19. The turbulent velocities required to account for the width of the lines were always modest, in the range $v_t \simeq 150 - 450$ km s^{-1}.

We have carried out a similar modelling analysis here, using the TLUSTY and SYNSPEC packages (Hubeny & Lanz 2017). As noted above, the narrow absorption features are present in all of our epochs – plateau, dip and echo outburst. However, the UV spectra during

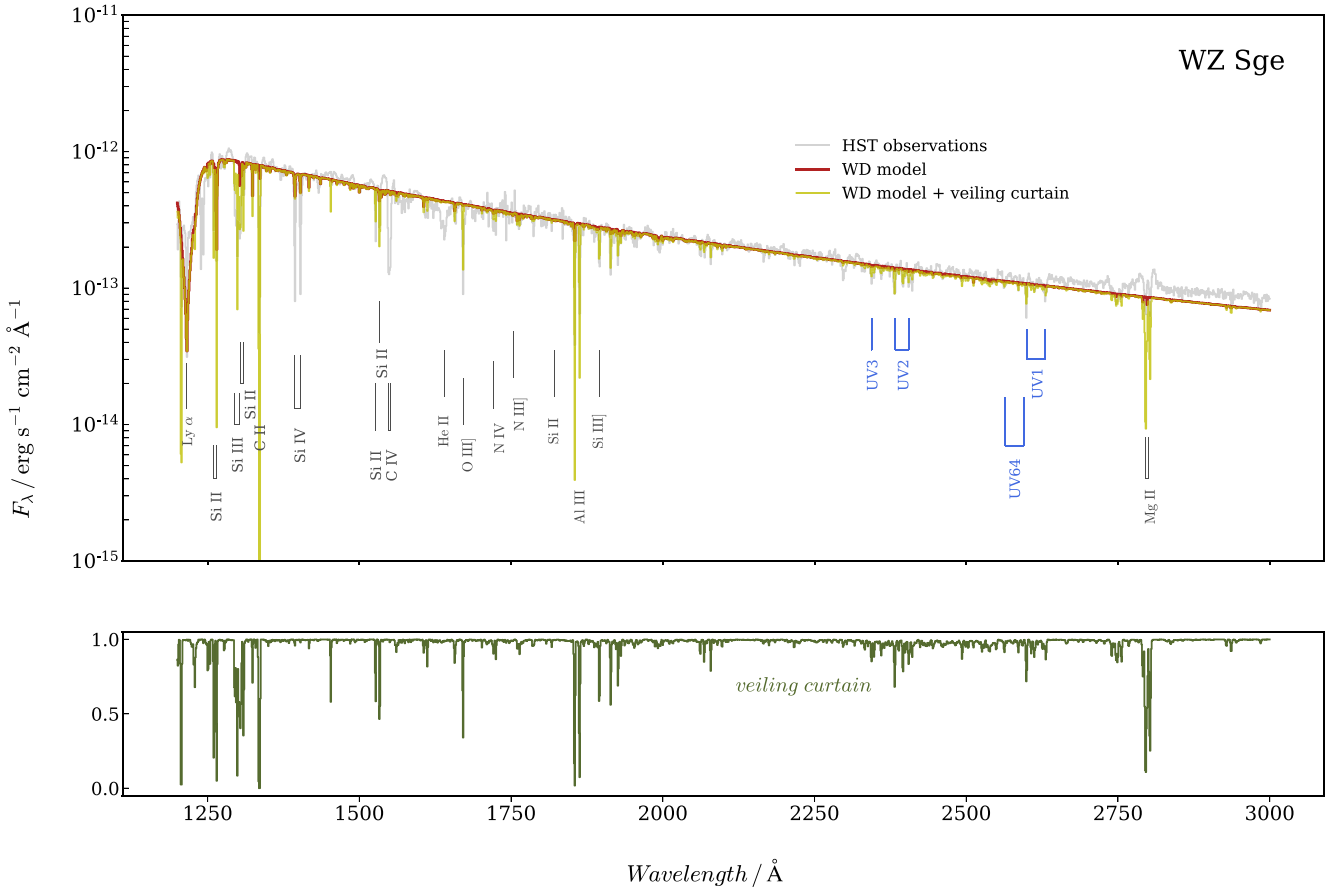

Figure 7. *Upper panel:* combined far- and near-UV spectrum, taken during the dip phase, of *WZ Sge* (grey) compared to the applied pure WD model (dark red) and the combination of the WD model and the veiling curtain (yellow). The most important lines are again identified at both parts of the spectrum. It is discernible that the addition of the veiling curtain is successful to produce the observing features. *Bottom panel:* demonstration of the absorbing veiling curtain (olive green) for comparison.

the plateau and echo-outburst phases are much harder to model, since they are dominated by disc emission and partially reprocessing in a disc wind (e.g. Knigge et al. 1997, 1998; Noebauer et al. 2010; Matthews et al. 2015). We therefore restrict our analysis here to the dip phase, where the accretion-heated WD is expected to be the dominant UV source. We intentionally keep our modelling simple and qualitative, since a fixed-density LTE slab model can only be expected to provide rough characteristic values for the physical parameters in the line-forming region. We begin by fitting a solar abundance, $\log g = 8.5$ (Steeghs et al. 2001), WD model to the far-UV through near-UV spectrum, taking care to exclude regions associated with strong absorption features that are clearly not associated with the WD. The resulting estimate of the WD temperature is $T_{WD} \simeq 27,300$ K, which is comparable to the estimate of $T_{WD} \simeq 29,100$ K obtained by Long et al. (2004) during the final dip phase in September 2001.

We then estimate the transmission spectrum of the veil by dividing the observed spectrum by the WD model. In order to remove any remaining large-scale trends that are not associated with absorption, we finally divide this spectrum by a highly smoothed version of itself. We use a very broad ($\simeq$500 Å) Savitzky–Golay filter for this purpose. We then fit this transmission spectrum with that expected for an LTE slab, varying the temperature (T), electron density (N_e), turbulent velocity (v_t) and column density (N_H).

Fig. 7 shows the resulting WD plus absorbing curtain fit to the data. The best-fitting LTE slab does a reasonable job of producing most of the observed features, and it is characterized by $T \simeq 17,200$ K, $\log N_e \simeq 15.7$, $v_t \simeq 120$ km s^{-1}, and $\log N_H \simeq 20.4$. As noted by Long et al. (2004), there is a strong degeneracy between T and N_e in LTE slab models, especially in the high-density, mostly ionized regime. If we follow them and fix $\log N_e = 11$, we obtain $T \simeq 14,400$ K, $v_t \simeq 260$ km s^{-1}, and $\log N_H \simeq 20.7$. Thus the exact values derived for the slab parameters should not be taken too literally, and some inferred quantities – e.g. the characteristic thickness of the slab ($H \simeq N_H/N_e$) – are particularly uncertain. However, the basic result is secure: the observed absorption features imply the presence of moderate temperature, high-density, low-velocity absorbing material along the line of sight. The temperature of this veil declines monotonically as the outburst progresses.

A new discovery here is that the same absorption features are present even in the disc-dominated plateau and echo-outburst phases. Hence the veil must be associated with a physical component that is present in all configurations throughout the outburst. During the plateau and echo-outburst phases, the ultraviolet emission comes mainly from the inner disc, a region spanning a few R_{WD}. Since at least part of this emission is absorbed, the veil is likely to have a lateral extent that is at least this wide. This strongly suggests that the veil is not associated with the WD itself, but is probably located in

the outer disc regions. *WZ Sge* is viewed fairly edge-on – its outer disc is partially eclipsed (Ritter & Schroeder 1979) – and absorption features associated with veiling material have also been seen in other high-inclination CVs. This includes both low-state systems, such as the 'Fe curtain' reported by Horne et al. (1994) in the eclipsing DN *OY Car*, and high-state ones, such as the absorption lines in the nova-likes *UX UMa* (Baptista et al. 1998) and *V348 Pup* (Froning, Long & Baptista 2003). Whether all of these veiling structures are physically related is an important open question. Understanding their physical nature should be a matter of priority.

3.3 If not a propeller, then what?

Where do these results lead us? As already noted in Section 1, complex outburst light curves like that shown in Fig. 1 are not expected in the standard DIM. Yet such light curves – with their 'dips' and echo outbursts – are a common signature, not just across the outbursts of *WZ Sge* itself (e.g. Patterson et al. 1981), but also across those of similar systems (see, e.g. Nakata et al. 2013; Kato 2015). Thus there must be an important missing ingredient in the standard DIM.

Several such ingredients have been proposed, usually based on modifications to the standard DIM. For example, Hameury, Lasota & Warner (2000b) and Buat-Ménard & Hameury (2002) suggested that rebrightenings may be associated with enhanced mass-transfer due to the irradiation of the secondary star during an outburst. Osaki, Meyer & Meyer-Hofmeister (2001) proposed that echo outbursts are connected to viscosity variations in the disc and Meyer & Meyer-Hofmeister (1994, 2015), argued that the evaporation of the inner parts of the accretion disc may be responsible. Hence the magnetic propeller scenario sketched by Campana et al. (2018) – which our analysis tends to rule out – is not the only game in town.

Recently, Hameury & Lasota (2021) have taken a new and comprehensive look at what modifications to the DIM are required in order to account for echo outbursts. They find that, in order to explain the full range of observed outburst phenomenologies, several conditions must be met: (i) the disc must be on the lower *stable* branch of the S-curve in quiescence, implying that outbursts are not triggered by the DIM itself, but by enhanced mass-transfer from the secondary, (ii) the disc must be truncated in quiescence, (iii) mass transfer during the outburst must be sustained 'externally' (e.g. by irradiation), beyond the duration the DIM would naturally support, (iv) stream overflow must be significant, depositing material closer to the WD than the outer disc edge. These are strong, but perhaps not unreasonable requirements. Now that the propeller model has been ruled out, these requirements, too, will need to be subjected to stronger observational tests.

4 SUMMARY AND CONCLUSIONS

We have tested the idea that the 'dip' in the super outburst light curve of *WZ Sge* stars is caused by a switch to a magnetic propeller state (Campana et al. 2018). Using time-resolved UV spectroscopy obtained just before, during and after the dip in the 2001 outburst of *WZ Sge* itself, we have constructed spectra representing both the constant and variable components in all three outburst phases. We then compared these spectra to the constant and variable components in the well-known magnetic propeller system *AE Aqr*. None of *WZ Sge*'s UV spectra show evidence for the distinctive broad emission line signatures seen in *AE Aqr*. This includes the spectra obtained for the dip phase, when the propeller should be active, and notably the variable component, which should isolate any time-dependent propeller signatures from the constant WD spectrum. Instead, all of *WZ Sge*'s spectra display more or less the same set of narrow, (mostly) low-ionization absorption features. All of this argues strongly against the propeller scenario in *WZ Sge*.

The narrow UV absorption lines in our spectra of *WZ Sge* are almost certainly the counterpart to the features noted by Long et al. (2004) later on in the same outburst. They cannot be formed in the atmosphere of the WD itself and therefore demand the existence of an absorbing 'veil' in the system. The temperature of this material declines over the course of the outburst – our modelling suggests $T \simeq 14,000-17,000$ K during the dip phase, compared to the highest value found by Long et al. (2004), $T \simeq 11,500$ K, in the interval between the final two echo outbursts. Importantly, the signature of the veil can be seen even during the disc-dominated plateau and echo-outburst phases. This suggests that the absorber is linked to a system component that is present throughout (at least) all of the super-outburst. An association with material in the outer disc seems likely, but the nature and origin of the absorber remain unknown.

We conclude by stressing the importance of resolving both of these mysteries: the peculiar outburst light curves and the nature of the absorbing veil. *WZ Sge* is the prototype of highly evolved accreting WDs, the most intrinsically abundant class of compact interacting binary systems. This, coupled with its brightness, orbital period and distance, makes it an ideal and important laboratory for accretion physics. We really should understand it better.

ACKNOWLEDGEMENTS

We would like to thank the anonymous referee for the constructive comments and suggestions, which improved the quality of the manuscript. We are also grateful to Mike Eracleous for providing us with his *AE Aqr* data products.

MG acknowledges support by the Mayflower scholarship in the School of Physics and Astronomy of the University of Southampton. NCS and CK acknowledge support by the Science and Technology Facilities Council (STFC), and from STFC grant ST/M001326/1.

This research has been conducted using MATPLOTLIB (Hunter 2007) and ASTROPY (Astropy Collaboration et al. 2018).

DATA AVAILABILITY

The UV observations of *WZ Sge* analysed at the current work are publicly available through the MAST: https://archive.stsci.edu/hst/. On the other hand, the *AE Aqr* data sets were provided to us after private communication with the author.

REFERENCES

Astropy Collaboration, 2018, AJ, 156, 123
Baptista R., Horne K., Wade R. A., Hubeny I., Long K. S., Rutten R. G. M., 1998, MNRAS, 298, 1079
Blinova A. A., Romanova M. M., Ustyugova G. V., Koldoba A. V., Lovelace R. V. E., 2019, MNRAS, 487, 1754
Buat-Ménard V., Hameury J. M., 2002, A&A, 386, 891
Campana S., Stella L., Mereghetti S., de Martino D., 2018, A&A, 610, A46
Echevarría J., Smith R. C., Costero R., Zharikov S., Michel R., 2008, MNRAS, 387, 1563
Eracleous M., Horne K., 1996, ApJ, 471, 427
Eracleous M., Horne K., Robinson E. L., Zhang E.-H., Marsh T. R., Wood J. H., 1994, ApJ, 433, 313
Evans I., 1993, FOS Instrument Science Report CAL/FOS-104
Froning C. S., Long K. S., Baptista R., 2003, AJ, 126, 964
Gaia Collaboration, 2021, A&A, 649, A1

Gänsicke B. T. et al., 2003, ApJ, 594, 443
Garnavich P., Littlefield C., Wagner R. M., van Roestel J., Jaodand A. D., Szkody P., Thorstensen J. R., 2021, ApJ, 917, 22
Godon P., Sion E. M., Cheng F., Gänsicke B. T., Howell S., Knigge C., Sparks W. M., Starrfield S., 2004, ApJ, 602, 336
Hameury J. M., 2020, Adv. Space Res., 66, 1004
Hameury J. M., Lasota J. P., 2021, A&A, 650, A114
Hameury J.-M., Lasota J.-P., Warner B., 2000a, A&A, 353, 244
Hameury J.-M., Lasota J.-P., Warner B., 2000b, A&A, 353, 244
Hernández Santisteban J. V., 2016, PhD thesis, University of Southampton
Horne K., Marsh T. R., Cheng F. H., Hubeny I., Lanz T., 1994, ApJ, 426, 294
Hubeny I., Lanz T., 2017, A brief introductory guide to TLUSTY and SYNSPEC (arXiv: 1706.01859)
Hunter J. D., 2007, Comput. Sci. Eng., 9, 90
Isakova P. B., Ikhsanov N. R., Zhilkin A. G., Bisikalo D. V., Beskrovnaya N. G., 2016, Astron. Rep., 60, 498
Ishioka R. et al., 2002, A&A, 381, L41
Kato T., 2015, PASJ, 67, 108
Knigge C., Long K. S., Blair W. P., Wade R. A., 1997, ApJ, 476, 291
Knigge C., Long K. S., Wade R. A., Baptista R., Horne K., Hubeny I., Rutten R. G. M., 1998, ApJ, 499, 414
Knigge C., Hynes R. I., Steeghs D., Long K. S., Araujo-Betancor S., Marsh T. R., 2002, ApJ, 580, L151
Lasota J., 2001, New A Rev., 45, 449
Lasota J. P., Hameury J. M., Huré J. M., 1995, A&A, 302, L29
Long K. S., Froning C. S., Gänsicke B., Knigge C., Sion E. M., Szkody P., 2003, ApJ, 591, 1172
Long K. S., Sion E. M., Gänsicke B. T., Szkody P., 2004, ApJ, 602, 948
Matthews J. H., Knigge C., Long K. S., Sim S. A., Higginbottom N., 2015, MNRAS, 450, 3331
Mauche C. W., Lee Y. P., Kallman T. R., 1997, ApJ, 477, 832
Meintjes P. J., Oruru B., Odendaal A., 2012, Mem. Soc. Astron. Ital., 83, 643
Meyer F., Meyer-Hofmeister E., 1994, A&A, 288, 175
Meyer F., Meyer-Hofmeister E., 2015, PASJ, 67, 52
Nakata C. et al., 2013, PASJ, 65, 117
Noebauer U. M., Long K. S., Sim S. A., Knigge C., 2010, ApJ, 719, 1932
Osaki Y., 1989, PASJ, 41, 1005
Osaki Y., 1995, PASJ, 47, 47
Osaki Y., 1996, PASP, 108, 39
Osaki Y., Meyer F., Meyer-Hofmeister E., 2001, A&A, 370, 488
Patterson J. et al., 2005, PASP, 117, 1204
Patterson J., 1979, ApJ, 234, 978
Patterson J., 1980, ApJ, 241, 235
Patterson J., 2001, PASP, 113, 736
Patterson J., McGraw J. T., Coleman L., Africano J. L., 1981, ApJ, 248, 1067
Patterson J., Richman H., Kemp J., Mukai K., 1998, PASP, 110, 403
Pearson K. J., Horne K., Skidmore W., 2003, MNRAS, 338, 1067
Ritter H., Schroeder R., 1979, A&A, 76, 168
Robinson E. L., Nather R. E., Patterson J., 1978, ApJ, 219, 168
Rosen S. R., Prinja R. K., Drew J. E., Mason K. O., Howell S. B., 1998, MNRAS, 299, 305
Sirk M., Bohlin R., 1986, FOS Instrument Science Report CAL/FOS-026
Smak J., 1993, AcA, 43, 101
Spruit H. C., Rutten R. G. M., 1998, MNRAS, 299, 768
Steeghs D., Marsh T., Knigge C., Maxted P. F. L., Kuulkers E., Skidmore W., 2001, ApJ, 562, L145
Steeghs D., Howell S. B., Knigge C., Gänsicke B. T., Sion E. M., Welsh W. F., 2007, ApJ, 667, 442
Welsh W. F., Horne K., Gomer R., 1998, MNRAS, 298, 285
Wynn G. A., King A. R., Horne K., 1997, MNRAS, 286, 436

This paper has been typeset from a TEX/LATEX file prepared by the author.